

A physical model for aftershocks
triggered by dislocation
on a rectangular fault

Rodolfo Console and Flaminia Catalli
Istituto Nazionale di Geofisica e Vulcanologia, Rome, Italy
e-mail: console@ingv.it, e-mail: catalli@ingv.it

May 2005
Submitted to Journal of Seismology

A bstract

We find the static displacement, strain and stress produced in an elastic medium by a finite size rectangular fault after its dislocation with uniform stress drop but a non uniform dislocation on the source. The time-dependent rate of triggered earthquakes is estimated by a rate-state model applied to a uniformly distributed population of faults whose equilibrium is perturbated by a stress change caused only by the first dislocation. The rate of triggered events in our simulations is exponentially proportional to the stress change, but the time at which the maximum rate begins to decrease is variable from fractions of hour for positive stress changes of the order of some MPa, up to more than a year for smaller stress changes. As a consequence, the final number of triggered events is proportional to the stress change. The model predicts that the total number of events triggered on a plane containing the fault is proportional to the $2=3$ power of the seismic moment. Indeed, the total number of aftershocks produced on the fault plane scales in magnitude as 10^M . Including the negative contribution of the stress drop inside the source, we observe that the number of events inhibited on the fault is, at long term, nearly identical to the number of those induced outside, representing a sort of conservative natural rule. Considering its behaviour in time, our model doesn't completely match the popular Omori law; in fact it has been shown that the seismicity induced closely to the fault edges is intense but of short duration, while that expected at large distances (up to some tens times the fault dimensions) exhibits a much slower decay.

Key Words: aftershocks, earthquake triggering, fault parameters, rate-and-state, Omori law.

1 Introduction

Studying the space-time interaction of earthquakes is important not only for the comprehension of the phenomenon of earthquakes, but also for its possible application in the mitigation of earthquake risk.

In this paper we aim to the physical modelling of the interaction between seismic events, seeking a relationship between the source parameters of an earthquake and the rate of all other

earthquakes that follow it, a phenomenon empirically and variably labelled with the names of seismic acceleration, foreshock and aftershock sequences, swarms, earthquake clustering, etc.

A purely statistical approach to this phenomenon exists with the name of "epidemic model" (Ogata, 1988; Ogata, 1998; Console et al., 2003). In the epidemic model each earthquake source is supposed capable of increasing the probability of new earthquakes according to a kernel space and time probability distribution decreasing from the source. The epidemic model is applicable not only to the aftershock phenomenon but also to the foreshock's. However, despite it provides an accurate statistical representation of earthquake interaction, the physical interpretation is ignored.

In order to formulate a more physical description of the clustered seismicity, we consider that seismic events modify the stress field around the causative fault. Our main goal in this work is to observe the spatio-temporal variation of the seismicity rate after an event introducing in the algorithm a rate-state model approach derived by Ruina (1983) and Diederich (Diederich, 1986; Diederich, 1992; Diederich, 1994). We aim to create a link between a physical modelling of the stress transfer and the epidemic model approach (see also Console et al. (2004)). Some recent studies put in evidence that sudden stress variations, even of small magnitude, can produce large variations of the seismicity rate. It is recognized as a phenomenon of triggering, rather than induction, on faults that are already subject to relevant stress. The seismicity rate increases in general where the stress change (called Coulomb Stress Change) is positive, according to the Coulomb model (Mendoza and Hartzel, 1988; Boatwright and Cocco, 1996; Stein et al., 1997; Gomberg et al., 2000). These studies were able to give a physical interpretation for earthquake interaction observed in specific cases, but were not suitable for the general application of the model in predictive way as it is necessary for the information contained in a seismic catalog. In particular, the Coulomb stress change criterion doesn't allow to model the hyperbolic time decay of the aftershock rate after a mainshock, known as the Omori Law. In this simple model all the next earthquakes would be advanced by a time which depends on the stress change and on the loading rate but doesn't depend on the physical properties of the fault. The experience shows that the Earth doesn't rather behave in this way. The most popular empirical description of the phenomenon is the Omori law, stating that the aftershock rate decays in time

as t^{-1} . Among the various theories modelling the Omori law, we have taken in consideration only the one that involves a particular constitutive behaviour of faults. Therefore, we have not considered, even without rejecting them in principle, other hypotheses that predict a time variation in stress, like the viscoelasticity and the diffusion of fluids in the medium. The rate-state model for earthquake nucleation seems capable of substantially explaining all the phenomenology. In this model slip doesn't occur instantaneously at the exceeding of a threshold stress as for the Coulomb-Amenon criterion, but follows a more complex time history with different phases. This time history depends on the physical properties of the fault too. The application of the rate-and-state model to the evolution of seismicity is not new, e.g., Toda et al. (1998) have used this model to predict the spatio-temporal seismicity rate after the Kobe earthquake. Other examples of application of the same model can also be found in the literature (Toda and Stein, 2000; Toda and Stein, 2002; Toda and Stein, 2003). Following the rate-state model it has recently been possible to simulate seismicity quite realistically, accounting for the rate of events induced by stress changes even at large distance from the inducing earthquake (Ziv, 2003; Ziv and Rubin, 2003).

Basing our work on the classical theory of the elasticity, we start from the formulation of the stress released by a rectangular fault with uniform stress-drop; then we apply the rate-state model (Dieterich, 1994), to the stress distribution, obtaining the complete time and space distribution of the seismicity induced by a given fault. It is important to remark that for present purposes we neglect the interaction between subsequent events, supposing that only the first event perturbs the stress field. We also neglect the effect of the free surface of the Earth. In this study we limit our interest to the behaviour of induced seismicity in space and time and its relationship with the fault's parameters. Because of the qualitative nature of this work we don't use the expressions derived, in a similar but more complex context, by Okada in 1992. The results of simulations are analysed to find out the scaling relationships existing between the free parameters of the model and the expected seismicity in a way that will allow the validation of the model by real observations.

2 Elastic model for a rectangular fault

Suppose that a fault is embedded in a homogeneous, isotropic, elastic medium where the stress tensor is uniform. At a particular moment, the fault slips generating an earthquake, and suppose that the earthquake fully releases the component of the traction parallel to the slip vector across the fault. We call (the stress drop) the uniform negative change of traction on the fault. It is well known that the slip distribution on a fault in similar conditions is not uniform. The slip distribution will satisfy the theory of the elasticity at the new equilibrium, and it will be zero on the edges of the fault. It is also well known that the shear stress on the fault plane outside the edges of the fault increases significantly.

The analytical solution for the slip distribution on a fault at the equilibrium doesn't exist except that for very simple geometries, such as a rectangular fault of constant width and infinite length (Knope, 1957) and for a circular fault (Keilis-Borok, 1959U das, 1999). As mentioned by Kostrov and Das (1998), the analytical solution is not known even for a geometry as simple as a rectangular shape of width W and length L . In the literature it is possible to find the computation of the stress field generated by an ideal rectangular fault with uniform slip in an infinite homogeneous space or semi-space (Chinnery, 1961Iwasaki and Sato, 1979Okada, 1985bOkada, 1985a). However, as mentioned above, this is not a situation of equilibrium fulfilling all the physical constraints imposed by the theory of the elasticity. For this reason, here we make use of a non uniform slip distribution that is approximately compatible with a uniform stress drop on the fault. The theoretical approach of this work has been made as simple as possible, still preserving the capability of modeling the stress transfer from seismic source to another.

To calculate the static displacement, stress and strain, we start from the components i of the static displacement vector $u_i^j(x)$ produced by an elementary force directed as the j axis in any point of an infinite, elastic, homogeneous and isotropic medium, known as the Somigliana Tensor. From the expressions valid for a single force source, those for a couple of forces of given moment are derived by differentiation with respect to the direction of the arm of the couple of forces. Then the expressions for a source represented by a double couple of forces are obtained by summing a pair of two coplanar couples orthogonal to each other. Once the expressions for the displacement are known, the strain e_{ij} and the stress σ_{ij} are computed by their definitions.

Our model of an extended source is drawn heuristically from that of a rectangular fault infinitely extending in one direction and that of a circular fault, and it is characterized by a slip distribution as:

$$u = \frac{u}{t} \frac{h}{\frac{W^2}{4} + \frac{x^2}{4} + \frac{L^2}{4} + \frac{y^2}{4}}; \quad (1)$$

defined for $W=2$ $x=W=2$ and $L=2$ $y=L=2$, where x, y are the coordinates on the fault plane whose origin is coincident with the center of the rectangle, u is the stress drop and t the shear modulus (rigidity) of the elastic medium. Equation (1) satisfies the condition of zero slip on the edges of the rectangle. The slip distribution is of a form very similar to that obtained numerically by discretization, except for the cases when one dimension is much larger than the other (Kostrov and Das, 1998). Its analytical form is similar to the solution for a circular fault. Moreover, for a fault of square shape ($W = L$) it achieves a seismic moment consistent with those obtained analytically for two circular faults, respectively inscribed and circumscribed to the square. Bonafede and Neri (2000) have shown that, when imposing a unidirectional traction release in the strike or dip direction, a minor component of slip is present, over the fault plane, even in the direction perpendicular to the released traction. In consideration of the qualitative character of this study, we have neglected this component.

For our numerical applications we discretize the continuous slip distribution of equation (1) with a set of point sources densely distributed on the fault. The more numerous are the point sources, the more accurate will be the approximation. Each element $(p; q)$ of the fault is characterized by its scalar seismic moment m_{pq} that, by the theorem of the representation is given by:

$$m_{pq} = u_{pq} A_{pq}; \quad (2)$$

where u_{pq} is the slip on the element $(p; q)$ and A_{pq} is its elementary area.

If $u_{pq}(x)$ is the displacement produced by the slip on the element $(p; q)$ in the point x , the displacement resulting from the combination of all the elements is computed by:

$$u(x) = \sum_{p=1}^{N^M} \sum_{q=1}^{N^N} u_{pq}(x); \quad (3)$$

where $u_{pq}(x)$ is computed by the relation valid for a point source of moment m_{pq} .

In our numerical simulations, we arbitrarily, but without lost of generality, suppose that the fault is on the $(x_1; x_3)$ plane. Following equation (1) the slip u_{pq} is written as:

$$u_{pq} = u_{max} \frac{r}{\frac{LW}{4}}; \quad (4)$$

where, in this case, x_{1p} and x_{3q} are the x_1 and x_3 coordinates of the element $(p; q)$ respectively, and:

$$u_{max} = \frac{p}{2} \frac{\frac{LW}{4}}{2}; \quad (5)$$

is computed through the other three fault parameters. These parameters are also connected to the scalar moment M_0 through the relations

$$M_0 = \overline{u} \frac{L}{W} = \frac{2}{16} u_{max} \frac{W}{L} = \frac{2}{32} (W/L)^{3/2} \quad (6)$$

where \overline{u} is the average slip on the fault.

The above mentioned theoretical approach has been implemented in a computer code which allows the user to choose among several options:

- Dimensions and stress drop, seismic moment, or magnitude of the fault;
- Slip direction (strike slip, dip slip, or tensional crack);
- Type of output: Displacement (3 components), and strain or stress (6 independent components).

The output values are given on a rectangular grid of points, whose orientation (horizontal, or vertical parallel to one of the co-ordinate axes), dimensions, and spacing are also selected by the user.

Figures 1 and 2 show two examples for the components of the stress field produced by a strike slip fault whose parameters are listed in Table 1. Note that these Figures show the stress change σ_{11} and not its absolute value.

Figure 1 clearly shows that the shear stress σ_{12} is maximum near the edges of the fault, in particular along the slip direction x_1 , and decreases with increasing the distance from the fault. Inside the fault σ_{12} is negative and approximately equal to σ_{11} .

3 The rate-state model

As already stated, we assume that the time-dependent behaviour of the seismicity triggered by a stress change in a population of faults is described by the rate-state model introduced by Ruina (1983) and Diederich (Diederich, 1986Diederich, 1992Diederich, 1994). According to Diederich (1994) the rate R of earthquakes due to a stress change is given by:

$$R = \frac{h \frac{r_i}{\frac{r_i}{\frac{t}{\tau_a}} + 1}}{\frac{1}{\frac{r_i}{\frac{t}{\tau_a}} + 1}} - r_i; \quad (7)$$

whose various parameters are defined in Table 2. Note that equation (7) doesn't predict the magnitude of the earthquakes, for the distribution of which we assume the classical Gutenberg-Richter frequency-magnitude relationship. However, both R and r refer to the number of earthquakes in a specific magnitude range.

The modelling of the space-time distribution of seismicity triggered by an earthquake is straightforward, introducing the expression for the stress change in equation (7). It should be noted that the component of the most favorable stress variation for triggering subsequent events is τ_{12} , the component that represents the shear stress on the plane of the fault; for this reason we introduce in this stress variation component and not a traction. We also make the assumption $\tau_{12} = \tau_x$. The meaning of this last assumption is that the primary earthquake doesn't change the long-term stress rate due to the tectonic driving forces in the environment.

It is easily understandable from (7) that the integral of R over infinite time diverges. This is due to the fact that the limit of R for $t \rightarrow \infty$ is the background rate r . We prefer to deal with the net triggered seismicity rate $R^0 = R - r$. The plot of R^0 versus time for different values of r is shown in Figure 3 (see also Diederich (1994)). It shows that the initial value of the triggered seismicity rate, immediately after the triggering event, is proportional to the exponential of the stress variation but the time period over which $R(t)$ is maximum and relatively constant decreases exponentially by the same factor for increasing stress change. This time period, in substantial agreement with Diederich (1994), can be obtained computing the intersection between $R^0(t=0)$ and the straight line corresponding to the limit of R^0 when $t \rightarrow \infty$. The

difference with Diederich (1994), as Figure 4 shows, is that we have preferred to make use of R^0 , rather than R , and we ignore the case $_ = 0$ which we judge not realistic. Such time period ranges from few hours for a variation $_ = 5 \text{ M Pa}$ to nearly one year for $_ = 1 \text{ M Pa}$. Figure 3 finally shows that the total duration of the triggered seismicity is the same but the shape of the decay is different for different $_$. The integration of R^0 over infinite time leads to the not completely trivial result that the total number of triggered events in an area of constant stress change is proportional to (Helmstetter et al., 2004):

$$\int_0^{\infty} R^0(t) dt = \frac{rt_a}{A} = \frac{r}{_} : \quad (8)$$

This relationship predicted by the friction model had been observed for Landers Aftershocks by Gross and Kisslinger (1997). We consider the integral over time of the triggered seismicity rate R^0 , once for a positive $_$, and then for a negative $_$ of the same size, and we sum the two functions. We obtain a quantity that initially has a positive increase and then tends back to zero (Figure 5). This result can be interpreted as a sort of conservative law of the seismicity, by saying that the total number of aftershocks generated in a place close to a fault can be balanced, at long range, by the total number of those events that are inhibited by the stress drop in a place internal to the fault if the stress drops are equal in absolute value.

For numerical applications it is necessary to define the value of the various parameters appearing in equation (7). Table 3 contains a list of values inferred from several geophysical considerations and used in our simulations. The reference seismicity rate, r , is a quantity that should be known experimentally for a given area, and it is related to the average strain rate $_$ of that area. We use for r a uniform value of four events of magnitude exceeding 3.0 per year per 1000 km^2 , and for $_$ a value of 5 K Pa per year. These are simplifications of the reality where r and $_$ are not geographically uniform. These parameters seem however reasonable for an area of moderate seismicity. The reason why r is expressed as a number of events per unit area and time is given below. The parameter A of the constitutive law has a value ranging from 0.005 to 0.015 obtained from laboratory experiments (Diederich, 1995). Generally, simulations that most nearly resemble earthquakes in nature were obtained with rather small values of A , near to $A = 0.001$. The value of A has been evaluated for different sequences of earthquakes

by several authors (Belardinelli et al., 2003; Stein, 1999). The parameter is the normal pressure on the fault (of the order of some tens of MPa). The characteristic time of aftershocks, t_a , depending on the other parameters through the relation $t_a = (A) = \dots$, in this context is of the order of several tens of years. This value is essential to model a long term triggered seismicity, because the effect of the stress change disappears completely after a time of the order of the double of t_a .

4 Application to a rectangular fault

Dieterich (1994) discussed in detail the case of a finite circular dislocation with uniform stress drop. In our simulations we have taken into consideration a vertical rectangular fault with horizontal slip in the x_1 direction, embedded in a homogeneous, isotropic, elastic medium. The values assumed for the fault parameters are again those reported in Table 1. Assuming a constant stress drop $\Delta \sigma$, equation (6) shows that the scalar seismic moment M_0 is proportional to the quantity $(W L)^{3/2}$, that can be considered a sort of equivalent source volume. Scaling W and L by a given factor, M_0 scales accordingly, and also the shape of the stress distribution in space scales by the same factor. Assuming that the background seismicity rate is given as the number of events per unit volume and time, and integrating over the space, we find that the number of events triggered by the earthquake is proportional to the cube of the linear dimensions, i.e. to the seismic moment M_0 , or to $10^{3/2M}$. In this study we make the different hypothesis that the aftershocks of an earthquake occur mainly on the fault plane. This hypothesis comes from the consideration that the fault plane is subject to the maximum shear stress and that it is a sort of plane of weakness where the triggered seismicity is more likely to occur. In this case, the number of triggered events would be proportional to $M_0^{2/3}$, or to $10^{M/3}$. If it was true, and neglecting other kinds of factors, one earthquake of given magnitude would have a number of aftershocks ten times larger than one earthquake of one magnitude unit smaller. Assuming, then, that the b value of the Gutenberg-Richter frequency-magnitude relation is equal to 1, it would follow that the earthquakes of a magnitude class produce the same number of aftershocks as the earthquakes of the magnitude class one unit smaller. This hypothesis is supported by the statistical analysis of real observations (Felzer et al., 2001; Yamamoto and Shimazaki, 1990; Utsu, 1969) and

will be used in the following of the paper.

A first group of simulations concerning the seismicity triggered by a fault as a whole have been performed to study the variation of the total number of triggered events (in space and time), N_{tot} , versus the main free source parameters: the stress drop $\Delta \sigma$, the linear dimensions L and the magnitude M . We assume that the magnitude M is proportional to the logarithm of the seismic moment M_0 (measured in N m) according to the Kanamori and Anderson (1975) relation:

$$\log M_0 = 9.1 + 1.5M : \quad (9)$$

Tables 4, 5 and (6) show the results obtained assigning a fixed value for one of the parameters at a time, and letting the others change. These simulations have been carried out by summation of the single contributions of the elementary cells constituting the area surrounding the fault. Only the seismicity triggered on the fault plane, but outside the fault edges, has been considered. Looking at Table 4 one can notice that, under our hypotheses, for a constant stress drop, the total number of triggered events increases about proportionally to the fault area LW . Theoretically it should be exactly proportional to the area of the source, but in the calculations there are numerical imprecisions due to the grid size approximations. These numerical simulations show, also, that the number of aftershocks is proportional to the $2/3$ power of the scalar seismic moment or to the exponential of the magnitude (10^M), in agreement with the above theoretical arguments. Table 5 clearly shows the proportionality existing between the stress drop $\Delta \sigma$ and N_{tot} , having fixed the linear dimensions of the fault. Furthermore, the results reported in Table 6 give credit to the hypothesis that, for a constant magnitude, the earthquakes of smaller linear dimensions generate a larger number of triggered events.

Let's mention, lastly, the results of a simple numerical test. We have theoretically shown that the total number of events triggered by a stress change $\Delta \sigma$ per unit area is, after a time much larger than the characteristic time t_a , identical to the number of events inhibited by a negative stress change $-\Delta \sigma$ on the same area. The numerical simulations reflect this idea in a more general way. In fact, if we take the total number of aftershocks produced in a time interval of 100 years by a fault of 100 km^2 on the portion of an area of 10^4 km^2 external to it, we find 353.2 events, while the same computation made including the negative contribution of the area

internal to fault itself gives only 15:6 (less than 5%). The idea of an overall null balance is, then, substantially met: the phenomenon of clustering doesn't change the long term seismicity rate of a large area. This is in contrast with the opinion that trigger zones produce many more shocks than are missing from the shadows (Toda and Stein, 2003). We nevertheless regard for Marsan (2003) that put in evidence the practical difficulty to observe in nature the lack of events (the quiescence) mainly when looking at weakly active regions and short timescales.

5 Temporal behaviour of the triggered seismicity

Let's now consider in more detail the dependence on time of the number of triggered events predicted by the present hypothesis. Kagan and Jackson (1991) and Diederich (1994) found, in their empirical works, that shallow aftershocks, above a given magnitude cut-off, decay globally (for different distance intervals) in about 10 years and this time decay appears to systematically decrease with increasing depth. In our model the behaviour in different zones depends on the different values of the stress changes, that decrease with the increasing distance from the edges of the fault. It can be then noted that the plateau of the plot of the seismicity rate in time (see Figure 3) has a duration that increases with the increasing distance from the source. This result depends on our assumption of considering only aftershocks on the mainshock fault plane. It can also be biased by the fact that we consider only the effect of static stress step and we ignore the interaction between events. In spite of that, we believe that our model can describe a behavior not so far from reality. Therefore we keep as our reference the model of fault given in Table 1.

As shown in Figure 6, in the close neighbouring of the fault (within 0.5 km from the perimeter of the fault), most of the aftershocks occur within one day after the occurrence of the inducing earthquake, and more than 1/3 of them occur already in the first hour. This is clearly not the case for further distance from the source: in the slice between 0.5 and 8.5 km from the fault, about half of the activity is exploited within about one year. The further we go apart from the source, the longer is the time interval necessary for the exploitation of the triggered activity. In fact, in the distant zone (from 20 to 100 km from the fault) most of

the triggered events occur longer than 20 years after the inducing earthquake. The behaviour shown in Figure 6 is illustrated also by the snapshots of the spatial distribution of the seismicity rate at different times. Figures 7, 8, 9 and 10 clearly show how the distribution of aftershocks resembles that of the stress change and how the time decay is different in the different slices.

We are now interested to know if the generalized Omori law is suitable to describe the temporal behaviour of $R^0(t)$ predicted by our model in every spatial slice and, in such case, by means of which free parameters. We refer to the generalized Omori law as to the formula describing the decay of aftershock rate after a mainshock (Utsu et al., 1995) through three free parameters a , c and p :

$$R^0(t) = \frac{a}{(c + t)^p} : \quad (10)$$

For this purpose we make use of an algorithm for the least squares best-fit of the sets of data reported in Figure 6 by the integral of (10) over the time:

$$y = \int_0^t R^0(t^0) dt^0 = a \frac{(c + t)^{1-p} - c^{1-p}}{1-p} : \quad (11)$$

The results obtained for the best-fit are shown in Table 7. It is evident that the values of the parameters obtained are quite different from case to case (for instance, the c parameter is extremely small for the slices closest to the fault edges), and that the standard deviation is larger for the slices that include the wider range of distances from the fault. These results show that the same set of parameters in equation (11) can not fit the synthetic values obtained for different zones. The observation that the Omori parameter varies spatially in real aftershocks sequences has been documented in a number of papers (Wiemer and Katsumata, 1999; Enescu and Ito, 2002; Wiemer, 2000; Wiemer et al., 2002; Wiemer and Wyss, 2002). Wiemer et al. (2002) reported a case of significantly different c values in the northern and southern Hector Mine aftershock volume, respectively. Enescu and Ito (2002) in their study of aftershock activity of the 2000 Western Tottori earthquake found c -values very close to 0 except for larger magnitude earthquakes, arguing that this feature could result from incompleteness of data, or might also reflect the complexity of the rupture process.

The situation is illustrated also by the plots of Figures 11 and 12, showing the graphical comparison between the synthetic data and the relative theoretical approximation for different slices.

6 Conclusions

The first step of our modelling, concerning the stress change in the medium following an earthquake, has given results comparable to those of previous papers as, for instance, Chinnery (1961), King and Cocco (2001), Belardinelli et al. (2003). This substantial agreement, though the simplifications introduced in this specific case of rectangular source, supports the validity of our methodology.

As to the interaction among seismic events, the application of the model of Diederich (1994) has shown how the total number of triggered events per unit area is proportional to the stress change. Nevertheless, the time constant by which the rate of events decreases has a large variability, ranging from a fraction of hour for a stress change of several MPa, up to tens of years for stress variations smaller than 1 MPa.

A first set of simulations carried out with a model of rectangular fault, based on the hypothesis that most of the aftershocks occur on the same plane of the fault, has shed light on the relationship between the main source parameters and the number of triggered events. The simulations lead to the conclusion that many earthquakes of small magnitude can produce, in total, a number of aftershocks comparable to that of fewer larger earthquakes. Our model predicts, in fact, that, for a constant stress drop, the number of triggered events is roughly proportional to the seismic moment at the power of 2=3, or equivalently to 10^M .

An important aspect of the model concerns the time-space behaviour of the triggered seismicity. The simulations show that the application of the rate-state model and equation (7) introduced by Diederich (1994) to the static model of stress change has as a consequence something more complicated than the conventional Omori law for the temporal decay of aftershock rate. In fact, the seismicity is expected to be intense (in accordance to the stress change,) and have a maximum constant value, close to the fault edges of the primary earthquake, but the time necessary for the starting of decay is shorter. On the contrary, the seismicity expected at larger distances (up to 10 times the linear dimensions of the fault) is weak, but the time necessary for the decay from the maximum value is longer (even some tens of years). We can conclude that the temporal behaviour of aftershock rate varies in space and this is theoretically because "c" increases with the distance from the fault edge. Moreover, the model predicts that

the total long term production of aftershocks, including wider areas, is not negligible respect to the short term production. In this respect, the regional background seismicity could be interpreted as a sort of noise, or memory, due to the superposition of the effect of many older earthquakes. The time decay described by the popular Omori law could be interpreted as an apparent average result of the contribution from the various areas on the plane containing the primary fault.

Let's list, in short, the most important results concerning the static effect of a dislocation, as following:

The number of triggered events is proportional to the area of the fault, for a constant stress drop;

the number of aftershocks is proportional to the 2=3 power of the static seismic moment, for a constant stress drop;

the logarithm of the total number of aftershocks scales linearly with the magnitude, for a constant stress drop;

the number of triggered events is proportional to the stress drop on the fault, if its linear dimensions are kept constant.

The rate-state model (Dieterich, 1994) used in our algorithm for the space distribution of the stress change produced by a dislocation on a rectangular fault, has allowed a partial justification of the Omori law. We outline the following main conclusions obtained from the simulations:

The seismic activity is very intense during the first few hours or days after the occurrence time of the primary earthquake, in the rectangular slice close to the edges of the fault;

The immediate decay of this intense activity is followed by a period of time during which the activity at larger distance (of the order of the linear dimensions of the fault) is nearly constant. For longer time (several years) the total number of triggered events in the external zone becomes comparable with that of the most internal one.

the number of events triggered over a long time scale at distances larger than the fault linear dimensions is significantly large;

the seismic activity inside the fault drops to negligible values at the occurrence of the primary earthquake and returns to normal values only after a time much longer than the characteristic time (several tens of years in our simulations); for a long time range the number of events inhibited inside the fault is comparable to that of the events triggered outside: the net balance can be considered null; the seismicity rate changes in space and time, but it doesn't have influence on the rate averaged over very large intervals of space and time.

We can conclude that the model here analysed, though its very simple conception, gives a physical justification both to the very popular phenomenon of short term earthquake clustering (aftershocks and foreshocks in strict sense) and to that of the long term induction, also observed in various occasions. Among the very crude approximations made in this model, two of the most important are (a) having neglected the dishomogeneity of the stress drop on the fault, and consequently the very complicated pattern of slip (this must certainly have influence on the aftershock pattern: some aftershocks may even occur inside the fault, where the gradient of slip is high); (b) having neglected the interaction between subsequent events. Nevertheless, we are confident that the refinement of the model and its validations with real catalogs will bring to even more interesting consequences.

Acknowledgments

We are grateful to Massimo Cocco for the stimulating discussions and his criticism which led to a significantly better version of the paper. We also would thank Tom Parsons for many useful suggestions to help make this paper clear.

Authors

R . C onsole,

Istituto Nazionale di Geoscienze e Vulcanologia,

via di V igna M urata, 605

00142, Rom e, Italy

mailto: console@ingv.it

phone:+ 39 06 51860417

fax:+ 39 06 5041181

F . C atalli,

Istituto Nazionale di Geoscienze e Vulcanologia,

via di V igna M urata, 605

00142, Rom e, Italy

mailto: cataldi@ingv.it

phone:+ 39 06 51860571

References

M. E. Belardinelli, A. Bizzarri, and M. Cocco. Earthquake triggering by static and dynamic stress change. *J. Geophys. Res.*, 108 (B 3):2135, 2003. doi: 10.1029/2002JB001779.

J. Boatwright and M. Cocco. Frictional constraints on crustal faulting. *J. Geophys. Res.*, 101 (10):13895{13910, jun 1996.

M. Bonafede and A. Neri. Effects induced by an earthquake on its fault plane: a boundary element study. *Geophys. J. Int.*, 141 (1):43{56, 2000. doi: 10.1046/j.1365-246X.2000.00074.x.

M. A. Chinnery. The deformation of the ground around surface faults. *Bull. Seism. Soc. Am.*, 51:355{372, 1961. doi: 10.1046/j.1365-246X.2000.00074.x.

R. Console, M. Murnu, and F. Catalli. Physical and stochastic models of earthquake clustering. submitted to *Tectonophysics*, 2004.

R. Console, M. Murnu, and A. M. Lombardi. Refining earthquake clustering models. *J. Geophys. Res.*, 108 (B 10):2468, 2003. doi: 10.1029/2002JB002130.

J. H. Diederich. A model for the nucleation of earthquake slip. *Geophys. Monogr. Ser.*, 37:36{49, 1986.

J. H. Diederich. Earthquake nucleation on faults with rate and state dependent strength. *Tectonophysics*, 211:115{134, 1992.

J. H. Diederich. A constitutive law for rate of earthquake production and its application to earthquake clustering. *J. Geophys. Res.*, 99 (18):2601{2618, feb 1994.

J. H. Diederich. Earthquake simulations with time-dependent nucleation and long-range interactions. *Nonlinear Processes in Geophysics*, 2:109{120, mar 1995.

B. Enescu and K. Ito. Spatial analysis of the frequency-magnitude distribution and decay rate of aftershock activity of the 2000 Western Tottori earthquake. *Earth Planet Space*, 54:847{859, 2002.

K . R . Felzer, T . W . Becker, R . E . Abercrombie, G . Ekström , and J . R . Rice. Triggering of the 1999 M W 7.1 Hector Mine earthquake by aftershocks of the 1992 M W 7.3 Landers earthquake. *J. Geophys. Res.*, 107 (B 9) 2190, 2001. doi: 10.1029/2001JB000911.

J. Gomberg, N M . Beeler, and M L . Blanpied. On rate-state and Coulomb failure models. *J. Geophys. Res.*, 105 (14):7857{7872, 2000.

J. Gomberg, N M . Beeler, M L . Blanpied, and P . Bodin. Earthquake triggering by transient and static deformations. *J. Geophys. Res.*, 103 (12) 24411{24426, oct 1998.

S. Gross and C . Kisslinger. Estimating tectonic stress rate and state with Landers aftershocks. *J. Geophys. Res.*, 102 (B 4):7603{7612, 1997.

R A . Harris. Introduction to special section: Stress triggers, stress shadows, and implications for seismic hazard. *J. Geophys. Res.*, 103 (12) 24347{24358, oct 1998.

A . Helmstetter, Y Y . Kagan, and D D . Jackson. Importance of small earthquakes for stress transfers and earthquakes triggering. submitted to *J. Geophys. Res.*, 2004.

T . Iwasaki and R . Sato. Strain field in a semi-infinite medium due to an inclined rectangular fault. *J. Phys. Earth*, 27:117{123, 1979.

Y . Y . Kagan and D . D . Jackson. Long-term earthquake clustering. *Geophys. J. Int.*, 104: 117{133, 1991.

H . Kanamori and D . L . Anderson. Theoretical basis for some empirical relations in seismology. *Bull. Seism. Soc. Am.*, 65:1073{1095, 1975.

V I . Keilis-Borok. On estimation of the displacement in an earthquake source and of source dimensions. *Annali di Geosc.*, 122,205{2,214, 1959.

D . Kilb, J. Gomberg, and P . Bodin. Aftershock triggering by complete Coulomb stress changes. *J. Geophys. Res.*, 107, 2002. doi: 10.1029/2001JB0002002.

G C P . King and M . Cocco. Fault interaction by elastic stress changes: New clues from earthquake sequences. *Adv. Geophys.*, 44:1{39, 2001.

L. Knopoff. Energy release in earthquake. Technical Report 90, Institute of Geophysics, University of California, U.S.A., 1957.

B.V. Kostrov and S. Das. Principles of Earthquake Source Mechanics. Cambridge University Press, 1998.

D. Marsan. Triggering of seismicity at short time scales following Californian earthquakes. *J. Geophys. Res.*, 108 (B5) 2266, 2003. doi: 10.1029/2002JB001946.

C. Mendoza and S.H. Hartzel. Aftershock patterns and main shock faulting. *Bull. Seism. Soc. Am.*, 78:1438{1449, 1988.

Y. Ogata. Statistical models for earthquake occurrence and residual analysis for point processes. *J. Amer. Statist. Assoc.*, 83:9{27, 1988.

Y. Ogata. Space-time point-process models for earthquake occurrences. *Ann. Inst. Statist. Math.*, 50:379{402, 1998.

Y. Okada. Internal deformation due to shear and tensile faults in an half-space. *Bull. Seism. Soc. Am.*, 82 (2):10181040, 1985a.

Y. Okada. Surface deformation due to shear and tensile faults in an half-space. *Bull. Seism. Soc. Am.*, 75 (4):1135{1154, 1985b.

A. Ruina. Slip instability and state variable friction laws. *J. Geophys. Res.*, 88 (B12):10,359{10,370, 1983.

R.S. Stein. The role of stress transfer in earthquake occurrence. *Nature*, 402:605{609, 1999.

R.S. Stein, A.A. Barka, and J.H. Dieterich. Progressive failure on the North Anatolian fault since 1939 by earthquake stress triggering. *Geophys. J. Int.*, 128:594{604, 1997.

S. Toda and R.S. Stein. Did stress triggering cause the large off-fault aftershocks of the 25 March 1998 Mw=8.1 Antarctic plate earthquake? *Geophys. Res. Lett.*, 27 (15):2301{2304, 2000.

S. Toda and R. S. Stein. Response of the San Andreas fault to the 1983 Coalinga-Nunez earthquakes: an application of interaction-based probabilities for Park field. *J. Geophys. Res.*, 107 (B 6) 2126, 2002. doi: 10.1029/2001JB000172.

S. Toda and R. S. Stein. Toggling of seismicity by the 1997 Kagoshima earthquake couplet: a demonstration of time-dependent stress transfer. *J. Geophys. Res.*, 108 (B 12) 2567, 2003. doi: 10.1029/2003JB002527.

S. Toda, R. S. Stein, P. A. Reasenberg, J. H. D. Deterich, and A. Y. Yoshida. Stress transferred by the 1995 M_w = 6.9 Kōbe, Japan, shock: Effect on aftershocks and future earthquake probabilities. *J. Geophys. Res.*, 103 (B 10) 24,543-24,566, 1998.

A. Udas. *Principles of Seismology*. Cambridge University Press, 1999.

T. Utsu. Aftershocks and earthquake statistics (i) { investigation of aftershocks and other earthquake sequences based on a new classification of earthquake sequences. *J. of Faculty of Science, Hokkaido Univ., Series V II (Geophysics)*, 3, 1969.

T. Utsu, Y. Ogata, and R. S. Matsuura. The centenary of the Omori formula for a decay law of aftershock activity. *J. Phys. Earth*, 43:1-33, 1995.

S. Wiemer. Introducing probabilistic aftershock hazard mapping. *Geophys. Res. Lett.*, 27 (20): 3405-3408, 2000.

S. Wiemer, M. Gerstenberger, and E. Hauksson. Properties of the Aftershock Sequence of the 1999 M_w 7.1 Hector Mine Earthquake: implications for aftershock hazard. *Bull. Seism. Soc. Am.*, 92 (4):1127-1240, 2002.

S. Wiemer and K. Katsumata. Spatial variability of seismicity parameters in aftershock zones. *J. Geophys. Res.*, 104 (B 6):13,135-13,152, 1999.

S. Wiemer and M. Wyss. Spatial and temporal variability of the b-value in seismic volumes. *Adv. Geophysics*, 45:259-302, 2002.

Y. Yamamoto and K. Shimazaki. Scaling relationship between the number of aftershocks and the size of the mainshock. *J. Phys. Earth*, 38:305-324, 1990.

A . Ziv. Foreshocks, aftershocks, and remote triggering in quasi-static fault models. *J. of Geophys. Res. (Solid Earth)*, 108:14,1{14,13, oct 2003.

A . Ziv and A . M . Rubin. Implications of rate-and-state friction for properties of aftershock sequences: Quasi-static inherently discrete simulations. *J. of Geophys. Res.*, 108:2051, 2003.
doi: 10.1029/2001JB 001219.

Figure captions

Figure (1): Shear stress τ_{12} parallel to the slip direction projected on the fault plane ($x_2 = 0.1$ km).

Figure (2): Shear stress τ_{12} parallel to the slip direction on a plane perpendicular to the fault.

Figure (3): Distribution of the triggered seismicity against time for different values of induced shear stress. The values of the parameters used are: $r = 2$ events=, $\tau = 3$ MPa, $A = 0.24$ and $\tau_0 = 5$ KPa.

Figure (4): Comparison between the behaviour of the rate against time in the two cases treated by Diederich (1994) and the case that we have selected in our study.

Figure (5): Distribution of the number of expected events in four different cases: (a) for a positive value of earthquake shear stress equal to 5 MPa, (b) for a negative value of it equal to -5 MPa, (c) the sum of (a) and (b) and (d) the integral of (c) over time. The values of r and t_a are fixed at 1.

Figure (6): Representation of the total number of induced events (on y-axis) in six different arbitrary slices (red, green and blue columns) around the principal fault after different intervals of time (x-axis). The distances of the limits of the slices are computed from the perimeter of the source and the reference magnitude in the simulation is 6.0. Histogram (a) represents

the distribution nearest the source at shorter intervals of time (the time scale is pure qualitatively). Histogram (b) represents the distribution farther from the fault at longer intervals of time.

Figure (7): Spatial distribution of the stress in the fault's plane ($x_2 = 0.1$ km) considering a magnitude $M = 6$.

Figure (8): Spatial distribution of the number of induced events at $t = 1$ hour.

Figure (9): Spatial distribution of the number of induced events at $t = 1$ year.

Figure (10): Spatial distribution of the number of induced events at $t = 100$ year.

Figure (11): Comparison between the temporal distribution of the cumulative number of induced events corresponding to synthetic data and the best fits obtained by the Omori law for the closer slices from the source.

Figure (12): Comparison between the temporal distribution of the cumulative number of induced events corresponding to synthetic data and the best fits obtained by the Omori law for the farther slices from the source.

Tables

Table 1: Source parameters used in numerical applications.

Parameter	Value	
Dimension of the fault	10 km	10 km
Spacing on the fault	0.05 km	
Dimension of the grid	20 km	20 km
Spacing on the grid	0.5 km	
Maximum slip	0.1 m	

Table 2: Constitutive parameters used in Diederich's relation.

Symbol	Description
r	reference seismicity rate
$\dot{\sigma}$	shear stressing rate
$\dot{\sigma}_r$	reference stressing rate
$\Delta\sigma$	earthquake stress change
A	fault constitutive parameter
σ_0	normal stress
t	time
t_a	characteristic time for seismicity to return to the steady state

Table 3: Values of the parameters used in the numerical applications of the model for induced seismicity.

Parameter	Value
r	4 events ($\text{yr}^{-1} 1000 \text{km}^2$)
α	5 K Pa
β	5 K Pa
A	0.008
	30 M Pa
t_a	48 yr

Table 4: Relation between fault parameters and aftershock production. The value of M is fixed at 4 MPa; the grid used in this computation has an area of 10^4 km^2 , the spacing on it is 0.5 km. The spacing on the fault is 0.05 km.

L [km]	W [km ²]	M	M ₀ [Nm]	N _{tot}
4	4.6	9.9	10^5	13.4
25	5.4	1.5	10^7	78.2
100	6.0	1.2	10^8	263.2
225	6.4	4.2	10^8	532.8

Table 5: Relation between fault parameters and aftershock production. The area of the fault is fixed at the value of 100 km^2 , the spacing is of 0.05 km; the grid used in the computation has an area of $17 \times 17 \text{ km}^2$, the spacing on it is of 0.5 km.

[MPa]	M	M ₀ [Nm]	N _{tot}
1	5.6	3.1 10^7	51.8
2	5.4	6.2 10^7	103.4
3	5.9	9.3 10^7	155.2
4	6.0	1.2 10^8	206.8
5	6.1	1.6 10^8	258.6

Table 6: Relation between fault parameters and aftershock production. The value of M is fixed at 6.0; the output grid is of $20 \text{ km} \times 20 \text{ km}$, the spacing is 0.5 km. The spacing on the fault is 0.05 km.

L [km]	W [km ²]	[MPa]	N _{tot}
4		510.7	overflow
25		32.7	597.6
100		4.1	223.2
225		1.2	107.8

Table 7: Results obtained for the best- t of the sets of data reported in Figure 6 by the relation (11). The symbol \pm indicates the standard deviation.

Slice	a [V^{p-1}]				c[V]				p	\pm
(0 0.5)km	3.24	0.17	0.37	10^7	0.2	10 ⁶	1.02	0.02	1.86	
(0 8.5)km	11.0	0.76	0.23	10^7	0.2	10 ⁶	0.91	0.032	9.16	
(0.5 8.5)km	83.7	70.0			3.1	1.96		1.44	0.19	3.3
(0 20)km	34.3	8.0	0.13	10^1	0.019		1.14	0.077	9.22	
(0 100)km	36.8	9.1	0.15	10^1	0.023		1.12	0.08	10.8	
(20 100)km	12.5	1.0	10.9	1.0	61.0	5.43		2.8	0.96	10^3
										0.45

Figure 1:

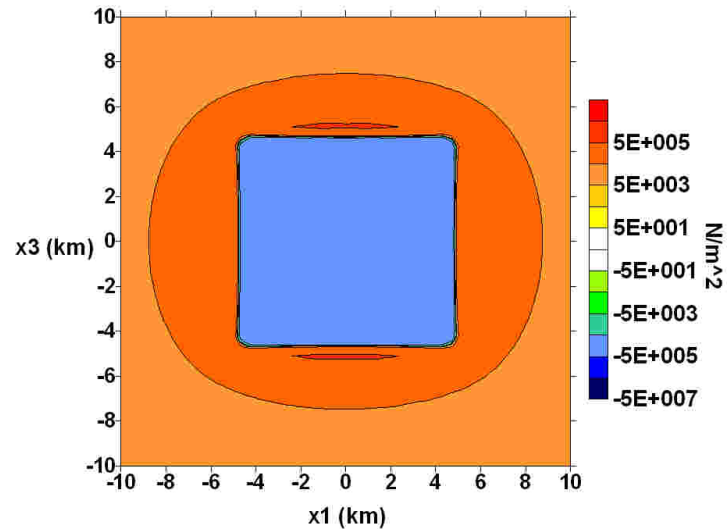


Figure 2:

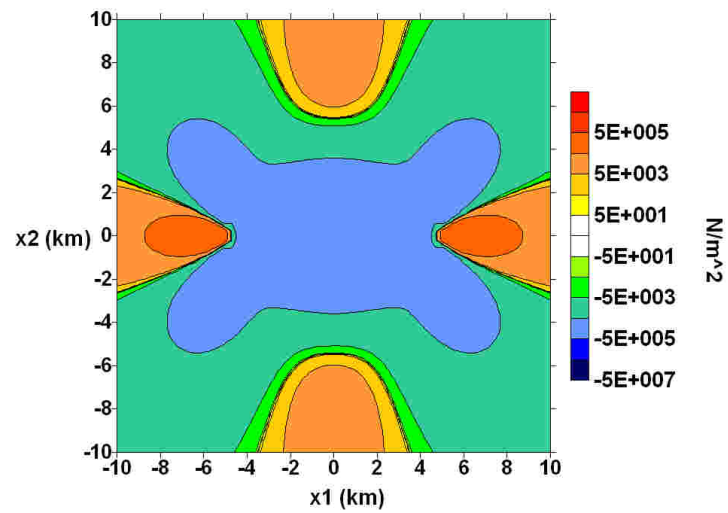


Figure 3:

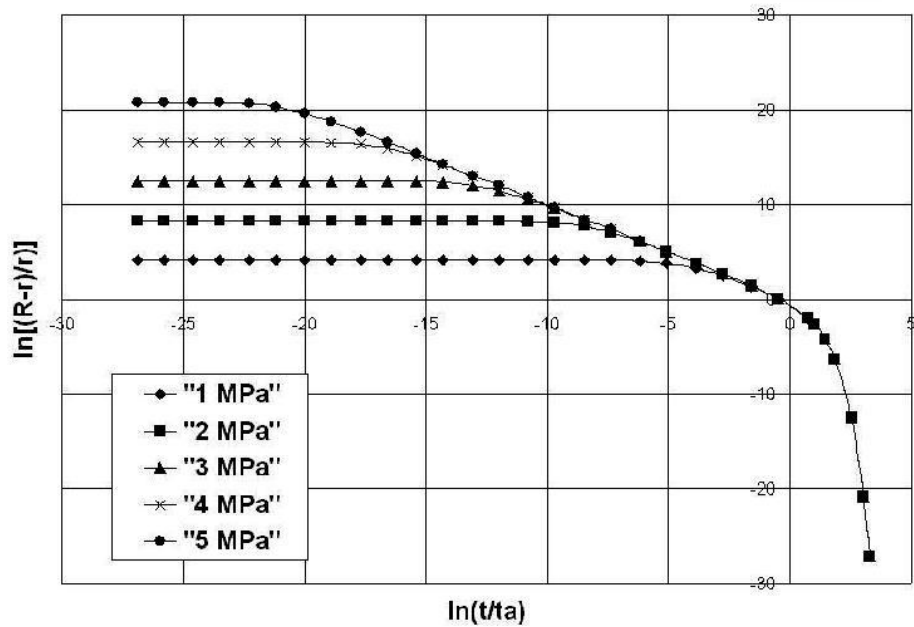


Figure 4:

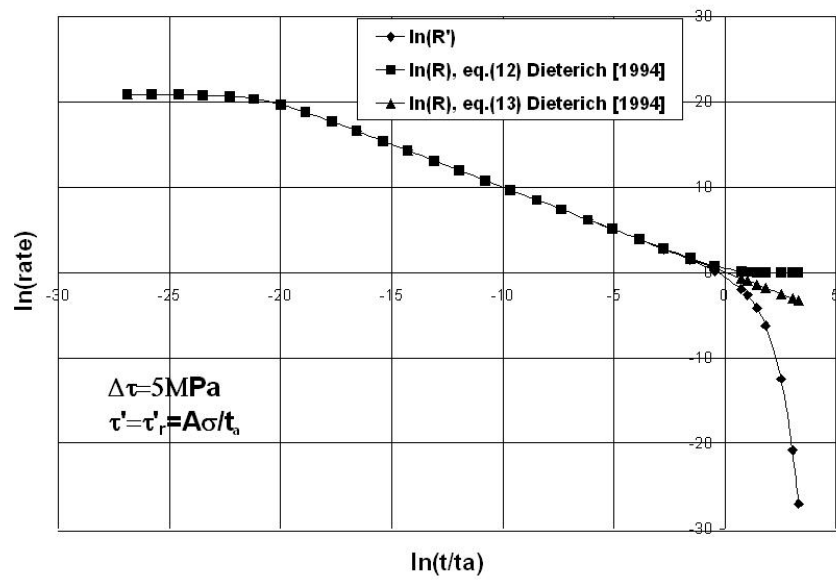


Figure 5:

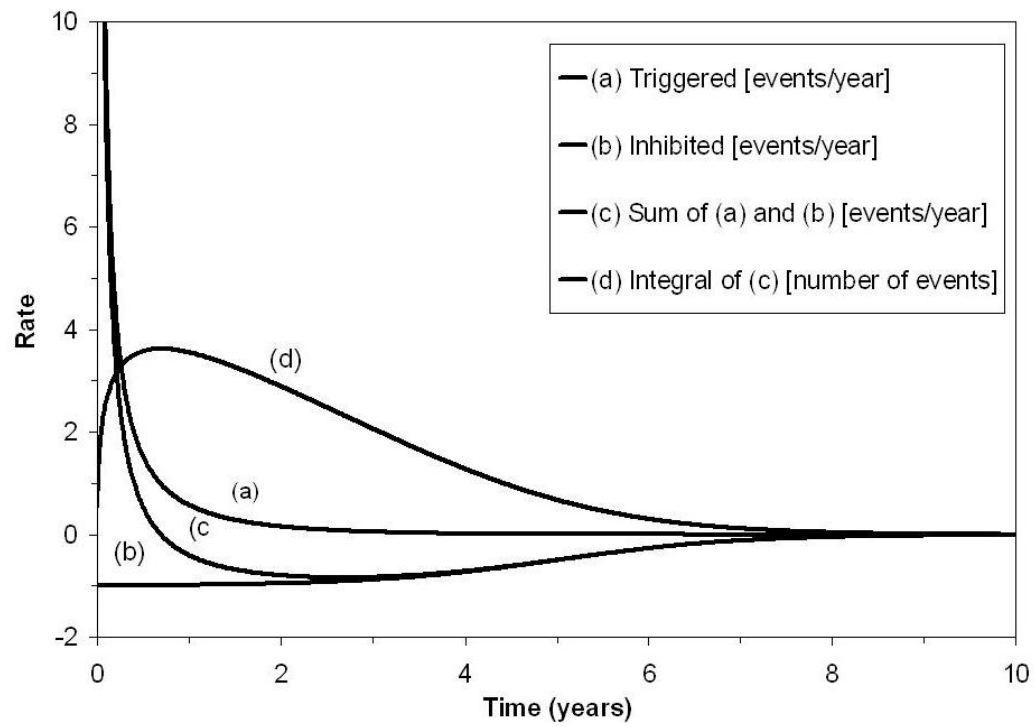
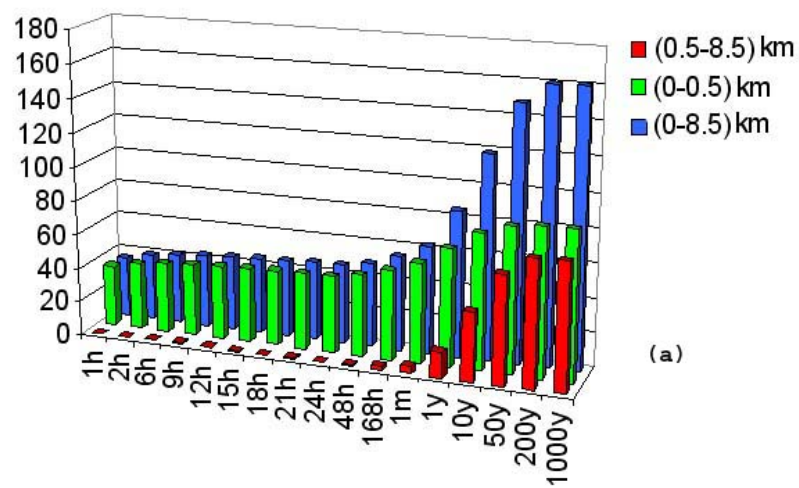
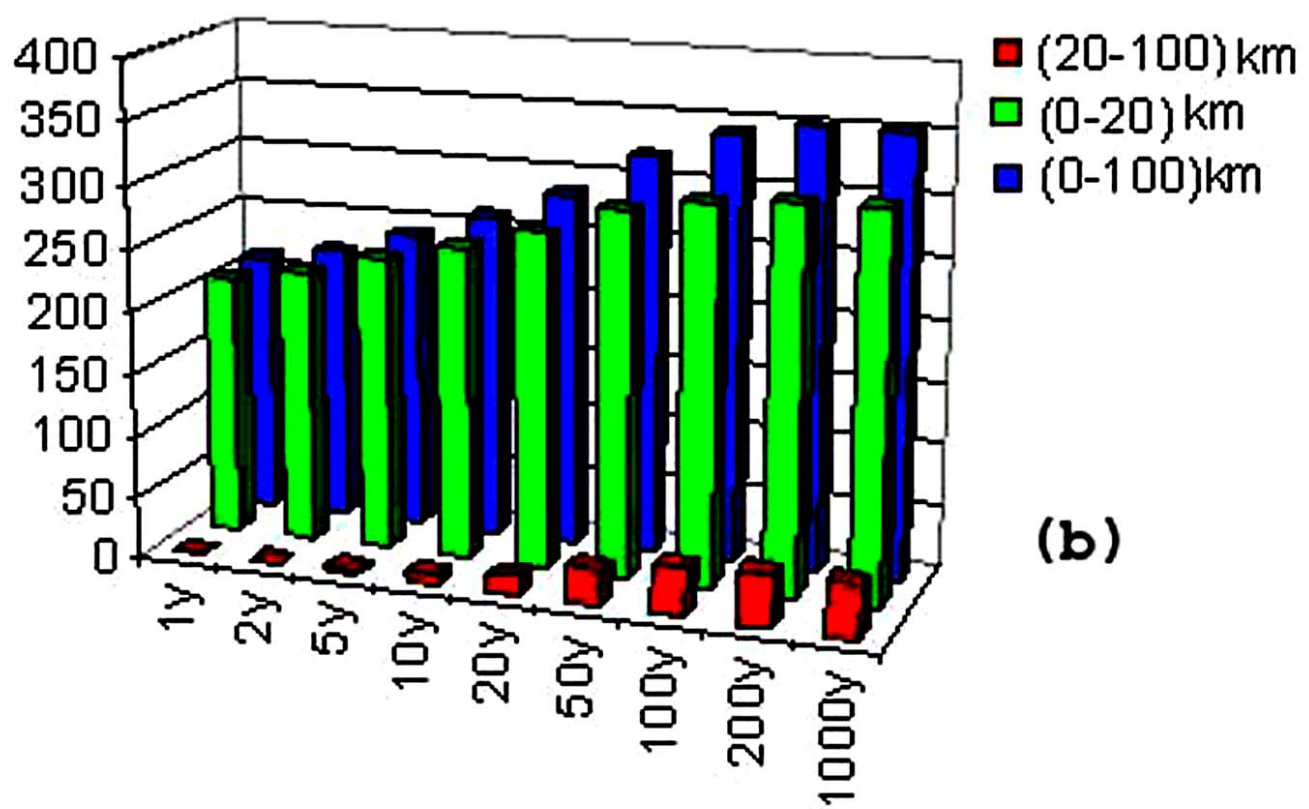


Figure 6:



(a)



(b)

Figure 7:

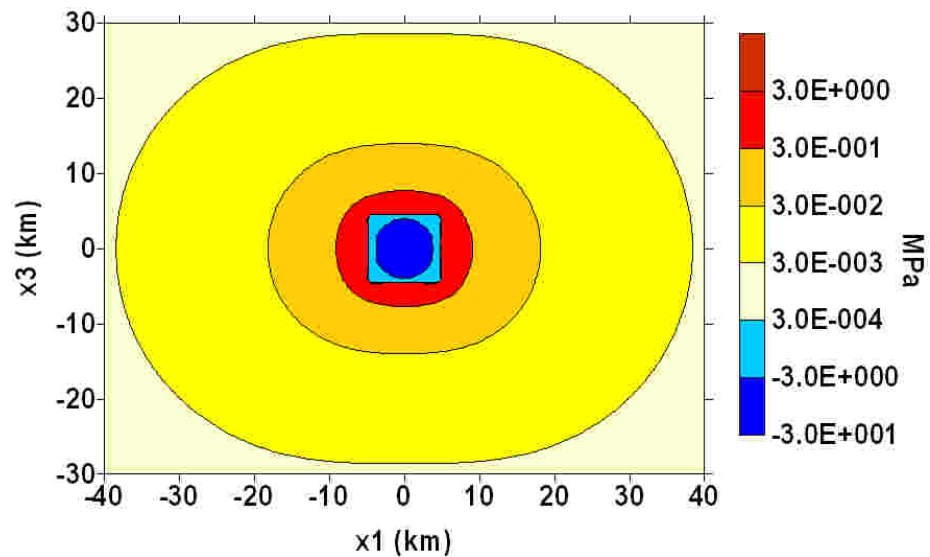


Figure 8:

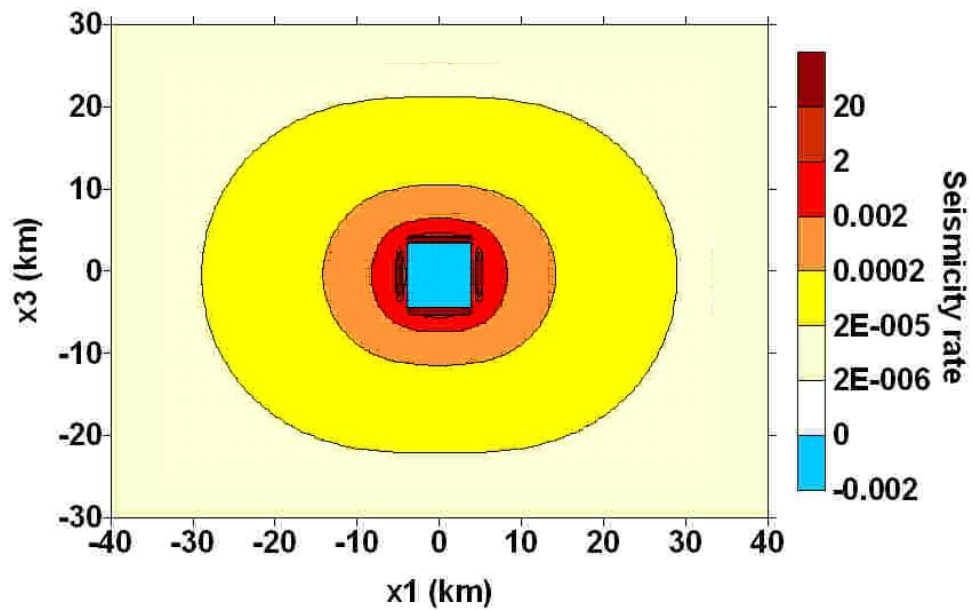


Figure 9:

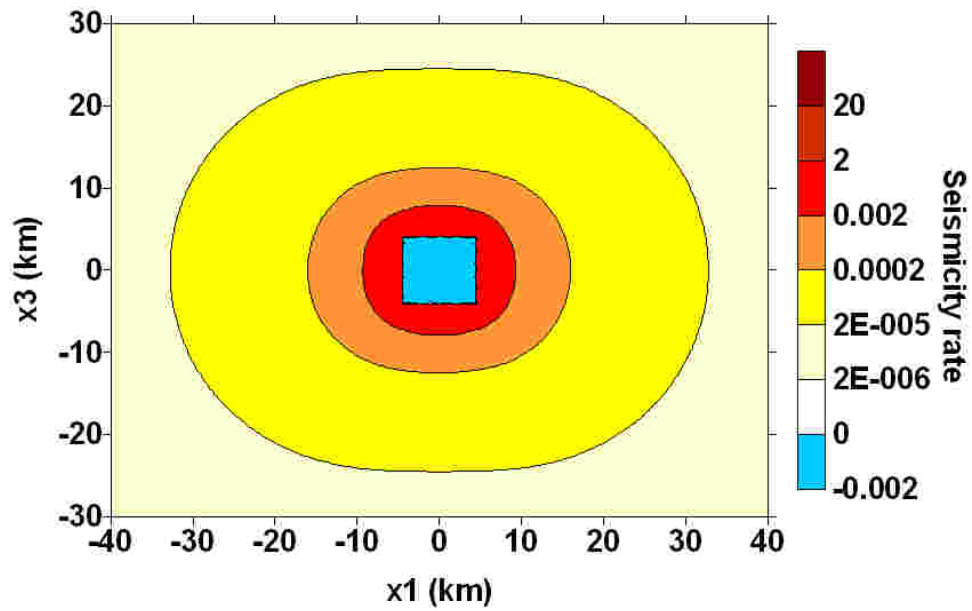


Figure 10:

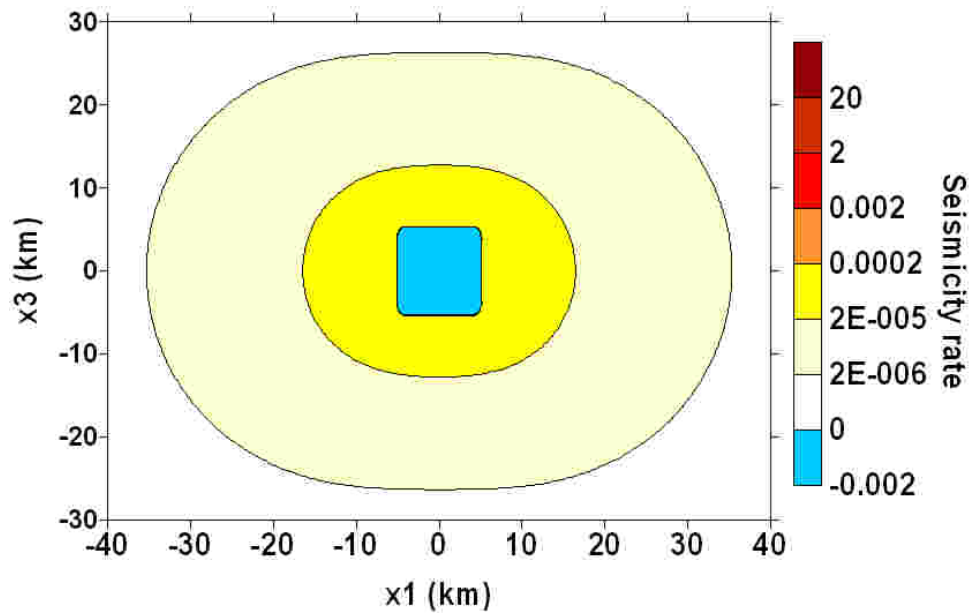


Figure 11:

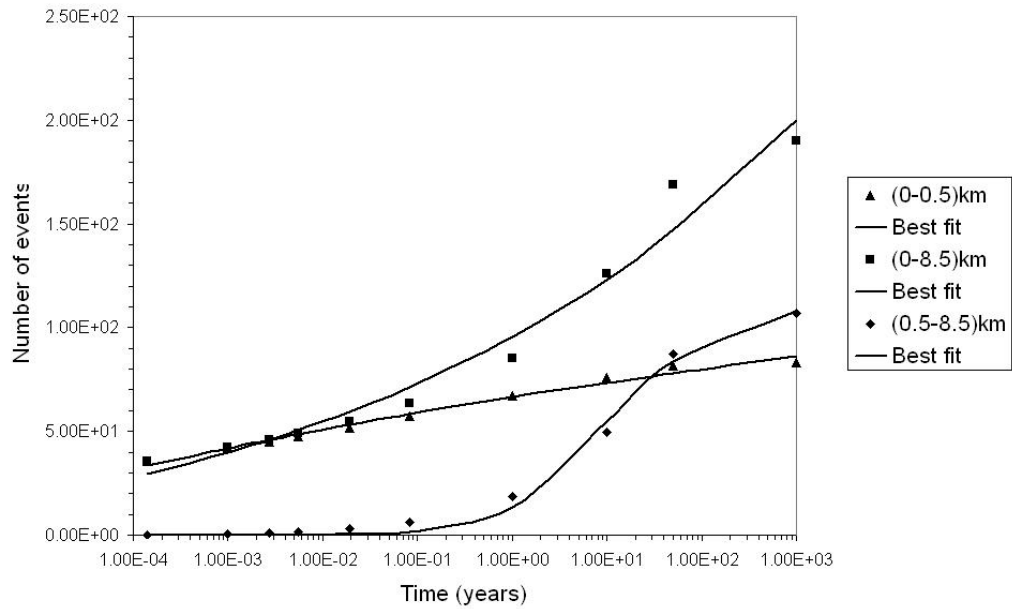


Figure 12:

